Journal of
Materials Chemistry A

Materials for energy and sustainability

Accepted Manuscript

This article can be cited before page numbers have been issued, to do this please use: K. Elbouazzaoui, C. A. Hall, K. Edström, J. Mindemark and D. Brandell, *J. Mater. Chem. A*, 2025, DOI: 10.1039/D5TA03403E.

ROYAL SOCIETY OF CHEMISTRY

rsc.li/materials-a

View Article Online
DOI: 10.1039/D5TA03403E

Polycarbonate-Based Solid-State Sodium Batteries with Inclusion of $NaAlO_2$ Microparticle Additives

Kenza Elbouazzaoui[1], Charles Aram Hall[1], Kristina Edström[1], Jonas Mindemark[1], Daniel Brandell[1,*]

[1]*Department of Chemistry – Ångström Laboratory, Uppsala University, Box 538, SE-751 21, Uppsala, Sweden*

**Corresponding author: Daniel.Brandell@kemi.uu.se*

Abstract

While polymer-based solid-state sodium batteries promise both safe operation and utilization of sustainable materials, they are held back by the insufficient ionic conductivity of the involved solid polymer electrolytes (SPEs). In this study, the conductivity and cation transference number are significantly improved through the construction of a composite polymer electrolyte (CPE) system based on poly(trimethylene carbonate) (PTMC) with sodium bis(trifluorosulfonylimide) (NaTFSI), combined with $NaAlO_2$ (NAO) ceramic filler for loadings ranging from 10 to 40 wt.%. The NAO-based CPEs shows the highest conductivity at 20 wt.% of NAO, with a Na^+ transference number of ~0.9 at 60 °C also being obtained for the same material, which is notably higher than for the NAO-free SPE. Solid-state batteries composed of a Prussian white cathode and a Na metal anode and employing these CPEs reach a cycling performance of ~100-150 mAh g^{-1} at a C/10 and 55 °C for more than 200 cycles without additives or plasticizers, thus opening the door to the potential exploration of CPEs for Na-based battery chemistries.

Keywords: Sodium-metal battery, Composite polymer electrolyte, Poly(trimethylene carbonate), Sodium aluminate

Introduction

As compared to lithium, sodium is a plentiful and cost-friendly element, which motivates the current interest in Na-based batteries.[1,2] Moreover, Na-ion batteries can be constructed without critical elements such as Cu, Co, Ni or P, or natural graphite, which render them potentially much more sustainable than the prevailing Li-ion counterparts. However, Na-ion batteries have safety concerns which are comparable to their Li-ion analogues, and their energy density is lower. Solid-state batteries (SSBs), in turn, can overcome the safety concerns related to both Li- or Na-ion batteries, and deliver higher energy densities thanks to the use of metallic Li/Na as the negative electrode.[3,4] The comparatively high energy density in Na-based SSB employing Na-metal anodes can also make them superior in terms of electrochemical performance in comparison with conventional Li-ion batteries, e.g. those based on $LiFePO_4$. Development of solid-state Na-metal batteries can therefore significantly improve the sustainability of battery technology, and contribute to reshaping the global clean energy landscape.

Both solid polymer electrolytes (SPEs) and solid inorganic electrolytes (SIEs) have been explored for Na-based SSBs.[5] Sodium β- and β''-Al_2O_3,[6,7] NASICON structures (e.g. $Na_3Zr_2Si_2PO_{12}$;

View Article Online
DOI: 10.1039/D5TA03403E

"NZSP") ,[8,9] and sulfides (e,g. Na_3PS_4, Na_3SbS_4)[10,11] constitute state-of-the-art Na-based SIEs, of which many can exhibit good ionic conductivity at room temperature (>10^{-4} S cm^{-1}) and high Na^+ transference number ($T_+ \sim 1$). However, implementing SIEs in solid-state Na batteries is technically challenging and results in high interfacial resistances due to the rigid solid/solid interfacial contacts.[12] This is a common disadvantage related to SIE-based batteries, almost regardless of the cell chemistry. SPEs can, on the other hand, present an efficient strategy to address this problem thanks to their flexibility and soft nature, enabling better interfacial contact with the electrodes. However, SPEs typically display shortcomings related to low ionic conductivity and transference number, limiting their applications in Na-based SSBs.

Equivalent to Li-based SPEs, poly(ethylene oxide) (PEO) has found potential also in Na-based SPEs. Qi et al., for example, fabricated a SPE made of PEO combined with sodium bis(fluorosulfonyl)imide (NaFSI) salt, which showed moderate ionic conductivity of 4.1×10^{-4} S cm^{-1} and a Na^+ transference number of 0.16 at 80 °C.[13] This combination of comparatively high SPE conductivity but poor cationic transference is typical for PEO-based SPEs. In contrast, polycarbonates have also been explored as SPEs for Na-based systems.[14] Sångeland et al. reported an SPE made of poly(trimethylene carbonate) (PTMC) with NaFSI salt, and showed that the ionic conductivity can reach >10^{-4} S cm^{-1}, with a moderate T_+ of 0.48 at 80 °C for the highest NaFSI concentration investigated.[15] A similar behavior was recently reported for polypropylene carbonate (PPC) with NaFSI, showing that an increase in the ionic conductivity can be achieved with high NaFSI salt content, reaching ~1 mS cm^{-1} at 80 °C at the highest investigated salt concentration of ~84 wt.%.[16]

Even though these highly concentrated SPE materials can display promising conductivity values, applications of SPEs in Na-based SSBs are likely more difficult to achieve due to limited mechanical properties. Moderate salt concentration will likely be necessary to achieve long-term battery operation, but these materials generally display limited conductivities. Alternative strategies to raise conductivity and transference numbers are therefore necessary. One such strategy is through combining a polymer and a ceramic material into a so-called composite polymer electrolyte (CPE). While extensive efforts have been dedicated to the development of CPEs for Li-based systems, the research into Na-based counterparts is much more limited.[17] In particular, CPE development has focused on the use of NASICON-type active (i.e., ion-conductive) ceramic fillers such as $Na_3Zr_2Si_2PO_{12}$,[18] $Na_{3.4}Zr_{1.8}Mg_{0.2}Si_2PO_{12}$,[19] $Na_{3.4}Zr_{1.8}Mg_{0.2}Si_2PO_{12}$,[20] and $Na_{3.4}Zr_{1.9}Zn_{0.1}Si_{2.2}P_{0.8}O_{12}$ in PEO-based SPEs.[21] It is noteworthy that while these reported Na-based CPEs exhibit better ionic transport and improved battery properties as compared to the pristine PEO-based SPEs, their performance is in many cases also largely dependent on the contribution arising from additives other than the ceramic fillers, such as liquid electrolytes or plasticizers.[17] Furthermore, much of these positive effects reported can be attributed to the decreased crystallinity of PEO or interfacial effects rather than from ion transport contributions from the actively conductive materials themselves. Passive (non-conductive) ceramic fillers should thereby be able to generate similar improvements in performance, but have not yet received equal attention. Using simple ceramic fillers such as SiO_2 and ZrO_2,[22–25] some success has been seen; e.g., Scrosati et al. reported a CPE based on a PEO:NaTFSI matrix with 5 wt.% SiO_2, delivering an ionic conductivity reaching ~1 mS cm^{-1} at 80 °C and a T_+ of 0.51 at 75 °C.[26] While this clearly indicates the potential

View Article Online
DOI: 10.1039/D5TA03403E

impact of implementing CPEs for Na systems based on low-cost and sustainable passive fillers, it also highlight the need for a better understanding of the functionality of the fillers in CPEs and their role and usefulness for Na-SSB development.

We have in recent work studied Li-based CPEs with the passive filler γ-$LiAlO_2$ incorporated into PTMC.[27] The material showed a large boost in conductivity as compared to the filler-free counterpart, a very high cationic transference number close to unity and also promising Li-battery performance. In this work, we study an analogous PTMC-based CPE platform with γ-$NaAlO_2$ ceramic filler as a direct Na-based counterpart. This constitutes the first exploration of non-polyether CPEs for Na-based SSBs. PTMC is chosen due to its amorphous nature, making it possible to directly see the effect of the ceramic fillers on the ionic conductivity without having the results obscured through changes in the degree of polymer crystallinity. Similar to the γ-$LiAlO_2$ CPE system, the addition of 20 wt.% γ-$NaAlO_2$ is shown to give a clear performance boost to the ionic conductivity and Na^+ transference number. Finally, the material is evaluated through galvanostatic charge–discharge cycling in battery cells comprising a Prussian white cathode and a Na-metal anode.

Experimental

Synthesis of $NaAlO_2$

γ-$NaAlO_2$ (abbreviated NAO) was synthesized following a sol–gel method. First, stochiometric amounts of $NaNO_3$ (Sigma Aldrich, ReagentPlus, > 99%), $Al(NO_3)_3 \cdot 9H_2O$ (Sigma Aldrich, ACS Reagent, >98%), and citric acid (Sigma Aldrich, ACS Reagent, >99.5%) were dissolved in deionized water, and stirred at room temperature. Afterwards, the solution was heated at 90 °C for 4–5 h until formation of a gel. The gel was thereafter transferred to a ventilated oven and kept at 120 °C for 12 h to ensure full dryness. The synthesis was finished by a heat treatment step at 900 °C for 4 h with a heating rate of 5 °C/min. The obtained white NAO powder was ground in a mortar before being transferred inside an Ar-filled glovebox.

Fabrication of SPE and CPE films

Polymer electrolyte films with and without fillers were fabricated employing a solution casting method reported previously.[28] First, PTMC with 30 wt.% NaTFSI was dissolved in acetonitrile. The solution was directly used for SPEs casting, while for CPEs, NAO particles were added within a range of 10 to 40 wt.% with respect to the polymer electrolyte matrix. The polymer:salt:particle mixtures were ball-milled at 25 Hz for 15 min to ensure good dispersion of ceramic particles in the polymer electrolyte matrix. The resulting slurries were thereafter poured into PTFE molds for vacuum drying at 60 °C for 60 h. Self-standing SPE and CPE films of 16 mm diameter and a thickness in the range 70–100 μm were obtained and stored inside an Ar-filled glovebox for further characterization. The superficial morphology of the CPE samples is illustrated by the photograph in **Figure S1.**

View Article Online
DOI: 10.1039/D5TA03403E

Materials characterization

The crystal structure of as-synthesized NAO and CPEs was investigated by X-ray diffraction (XRD) on a Bruker D8 Advance diffractometer using Cu Kα radiation (λ_1 = 1. 1.54060 Å and λ_2 = 1.54444 Å). XRD patterns were acquired over a 2θ range of 10–80° with a step size of 0.02. Lattice parameters of $NaAlO_2$ were determined via a Pawley fit using TOPAS V6.[29] The peak shape was determined using a NIST 1976b standard (Al_2O_3). The $P4_12_12$ (92) space group was used for fitting. Fourier transform infrared (FTIR) spectroscopy was carried out on a PerkinElmer Spectrum One FT-IR spectrometer equipped with a ZnSe crystal attenuated total reflectance (ATR) setup. The FTIR spectra were recorded from 4000 to 650 cm^{-1} with a resolution of 4 cm^{-1} on the SPE and CPEs. The NAO particle size distribution, particle shape and particle distribution in the composite electrolyte films were characterized by scanning electron microscopy (SEM) carried out on a Zeiss SEM instrument. Top view (NAO powder) and cross-section (CPE film) SEM images were acquired with an applied acceleration voltage of 3 and 2 kV, a 5 and □8 mm working distance, respectively, using an InLens electron detector for both NAO powders and CPE films.

Cell assembly and electrochemical characterization

The total ionic conductivity was measured on a Schlumberger SI 1260 Impedance/Gain-Phase Analyzer with the SPE and CPE materials sandwiched between two stainless steel electrodes in a CR2025 coin cell configuration. The measurements were carried out from 7 MHz to 100 mHz at an AC amplitude of 10 mV, while increasing the temperature up to 90 °C in 10 °C intervals. The assembled cells were annealed at 90 °C for 1 h one day before the measurement to improve the interfacial contact.

Cationic transference numbers were investigated electrochemically employing the Bruce–Vincent method[30] on a BioLogic SP-240 potentiostat at 60 °C. Before and after applying a potentiostatic polarization of 10 mV, the cell impedance was measured from 7 MHz to 100 mHz. Symmetrical pouch cells for the measurements were assembled using SPE/CPE films of 16 mm in diameter sandwiched between two 13 mm sodium disks. The cells were kept at 60 °C overnight prior to measurements. The sodium transference number T_+ was determined from Equation 1:

$$T_+ = \frac{I_{SS}(\Delta V - I_0 R_0)}{I_0(\Delta V - I_{SS} R_{SS})} \quad (1)$$

Prussian white ($Na_xFe[Fe(CN)_6]$) powder from Altris was used as received as cathode active material. A full characterization of this material can be found in Ref. [31]. Positive electrodes were prepared by mixing Prussian white in a water-based slurry with a carboxymethyl cellulose (CMC) binder and conductive carbon additive (Enasco 250P). The slurry composition was 85:10:5 (w/w) for Prussian white, carboxymethyl cellulose and conductive additive. Slurries were cast on carbon-coated aluminum foil at 100 µm thickness (wet coating), resulting in an areal mass loading of ~1 mg cm^{-2}. These were punched to 13 mm diameter electrodes.

Electrochemical characterization was performed using a pouch cell configuration with metallic sodium as the negative electrode. Prior to assembly, the Prussian white electrodes were dried under vacuum at 170 °C for 15 h inside an Ar-filled glovebox (O_2 and H_2O <0.5 ppm). Sodium electrodes were prepared in a glovebox from sodium cubes by pressing cleaned Na onto aluminum foil using

View Article Online
DOI: 10.1039/D5TA03403E

a hydraulic press. Current collectors in the pouch cells were made of Al foil. Pouch cells were assembled with the CPE (16 mm in diameter) sandwiched between a cathode of 13 mm diameter and a sodium disk of 15 mm diameter. Galvanostatic cycling tests were carried out with an ARBIN BT-2043 on the lab-scale pouch cells. Cycling was performed at C-rates calculated based on a practical capacity of ~150 mAh g^{-1} for the Prussian white material. Practically, the cycling was carried out initially from a C-rate of C/10 up to 5C within a voltage window of 2.0 – 4.0 V at room temperature and 55 °C

Results and Discussion

$NaAlO_2$ is an inorganic compound usually employed for different industrial applications such as water softening, waste water treatment, or as a catalyst for biodiesel production.[32,33] $NaAlO_2$ can exist in two isostructural forms: β and γ, and the phase transformation from β (low temperature phase) to γ (high temperature phase) occurs around 743 K. Stabilization of the γ-phase at room temperature can be enabled after rapid cooling.[34,35] The crystal structure of $NaAlO_2$ can be described as similar to $NaFeO_2$, consisting of a framework composed of NaO_4 and AlO_4 corner-sharing tetrahedra through oxygen atoms.[36,37] It can be expected that γ-NAO is an analogous compound to γ-$LiAlO_2$ (LAO) in terms of its intrinsic crystallographic fingerprint, and can therefore display a similarly preferable surface structure for promoting cationic transport as its Li-based counterpart. Looking at the X-ray diffraction (XRD) pattern of the as-synthesized NAO and LAO, shown in **Figure 1 and S2**, it is clear that both materials display formation of the same γ crystalline phase, confirmed from the appearance of the characteristic diffraction peaks observed at 2θ ~ 22.11°, 24.31°, 28.13°, 33.20°, and 34.61°, which can be attributed to the (101), (110), (111), (102), and (200) reflections, respectively. This confirms the successful synthesis of γ-$NaAlO_2$, isostructural with γ-$LiAlO_2$.[38] As can be seen in the SEM micrographs in **Figure S3**, the synthesized powders were of a hierarchical structure, forming micron-sized larger particles with irregular shapes.

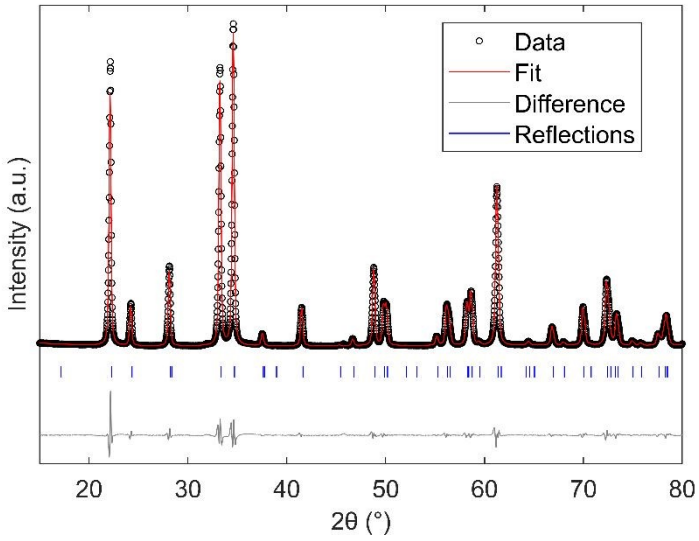

View Article Online
DOI: 10.1039/D5TA03403E

Figure 1. Pawley refinement pattern of NAO. Experimental XRD profile, calculated profile and difference plots are indicated by dotted line (black), solid lines (red) and bottom black line respectively. All possible Bragg positions are shown by vertical lines (blue).

As displayed in **Table 1**, both Na and Li aluminates share the same $P4_12_12$ space group and have similar unit cell parameters, indicating that NAO crystallizes in the same way as LAO with a tetragonal symmetry.

Table 1. Crystallographic data including the unit cell parameters of $NaAlO_2$ in the γ-phase. Data was determined from refining the experimental XRD pattern (**Figure 1**).

	γ-$NaAlO_2$
Space group	$P4_12_12$ (92)
Unit cell parameters	$a = b = 5.16558 \pm 0.00009$ Å $c = 6.2811 \pm 0.0001$ Å $\alpha = \beta = \gamma = 90°$
Unit cell volume	$V = 167.599 \pm 0.007$ Å^3

The filler-free PTMC:NaTFSI SPE and PTMC:NaTFSI:NAO CPEs were prepared by a solution casting method, which has been used previously to fabricate CPEs with LiTFSI and $LiAlO_2$.[27] As described in the experimental section, an additional step of ball-mill mixing is needed to ensure homogeneity of the solution containing PTMC, NaTFSI and NAO particles. Therefore, it is essential to verify that all CPE components are structurally stable, and also that the addition of NAO particles did not change the characteristics of the polymer matrix. As shown in **Figure 2a,** all characteristic peaks of NAO particles are maintained for all CPEs from 10 up to 40 wt.%, indicating that the γ-phase is indeed stable and does not undergo any structural changes. Since PTMC is a fully amorphous polymer, no effect of reducing the polymer crystallinity is expected after incorporating NAO particles. The chemical fingerprint of the polymer matrix was examined by FTIR spectroscopy. **Figure 2b** depicts the FTIR spectra of electrolytes with and without NAO particles, also including peak assignments of the C=O stretch vibration. Since PTMC is a polycarbonate, it shows the characteristic C=O stretch at approximately 1740 cm^{-1}, which shifts towards lower wavenumbers when it coordinates to cations, *i.e,* in this case sodium ions.[39] This behavior is also observed for the system composed of PTMC with NaTFSI salt, and is unchanged after incorporating NAO ceramic filler regardless of loading. Additional peaks in the fingerprint region are much more difficult to clearly assign and this region is also largely unaffected by the addition of the NAO particles.

View Article Online
DOI: 10.1039/D5TA03403E

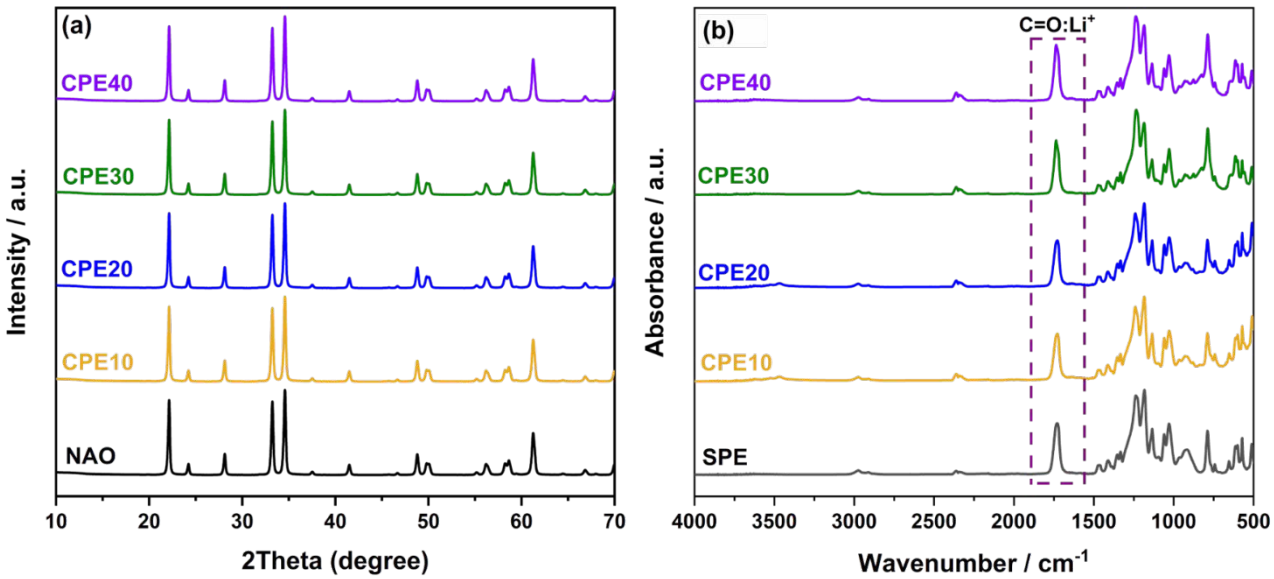

Figure 2. (a) XRD patterns of the as-synthesized NAO particles and PTMC-based CPEs; (b) FTIR spectra of the filler-free SPE and CPEs (NAO loadings from 10 to 40 wt%).

The fabricated SPE and CPEs were assembled in coin cells with blocking stainless steel electrodes to evaluate the influence of adding NAO ceramic filler on the ion conduction properties of the PTMC:NaTFSI electrolytes. The temperature dependence of the ionic conductivity is displayed in **Figure 3a,** and exhibits the typical Vogel–Fulcher–Tammann (VFT) type of behavior expected of amorphous polymers where the ionic transport is coupled to the polymer segmental motion. The ionic conductivity of the filler-free SPE is in good agreement with data previously reported for the same PTMC:NaTFSI system at approximately the same NaTFSI salt concentration.[40] Upon incorporating 10 or 20 wt.% of NAO particles, the conductivity significantly increases to higher values within the entire investigated temperature range, but without any changes in the shape of the curves. This indicates that similar ion transport mechanisms are effective in all samples, also after addition of NAO particles, and is consistent with the formation of uniform films with dispersed particles (see **Figure S4**). Above 20 wt.% ceramic filler loading, the ionic conductivity decreases. This behavior was observed also for PTMC:LiTFSI:LAO CPEs, and has been attributed to particle agglomeration; leading to less polymer–ceramic interface area, to tortuosity effects and to a dilution of the conductive SPE phase.[27] Nevertheless, it is interesting that the ionic conductivity above 20 wt.% of NAO still remains higher than the conductivity of the filler-free reference SPE. In comparison with other solid-state Na-conductors, however, the total ionic conductivity is not exceptionally high (see **Table S1**); this is a reflection of the use of PTMC as the polymer host.

The increase of the ionic conductivity by one order of magnitude should be considered significant. This also reflects a similarity between the LAO and NAO ceramic fillers for Li- and Na-based systems, respectively. Therefore, it is likely that the reasons behind the improved ionic conductivity for NAO-based CPEs are similar as for LAO-based CPEs; i.e., an accumulation of anions at the

View Article Online
DOI: 10.1039/D5TA03403E

particle surfaces that create additional ion transport pathways along the polymer–ceramic interfaces, combined with an improved ion–ion separation.

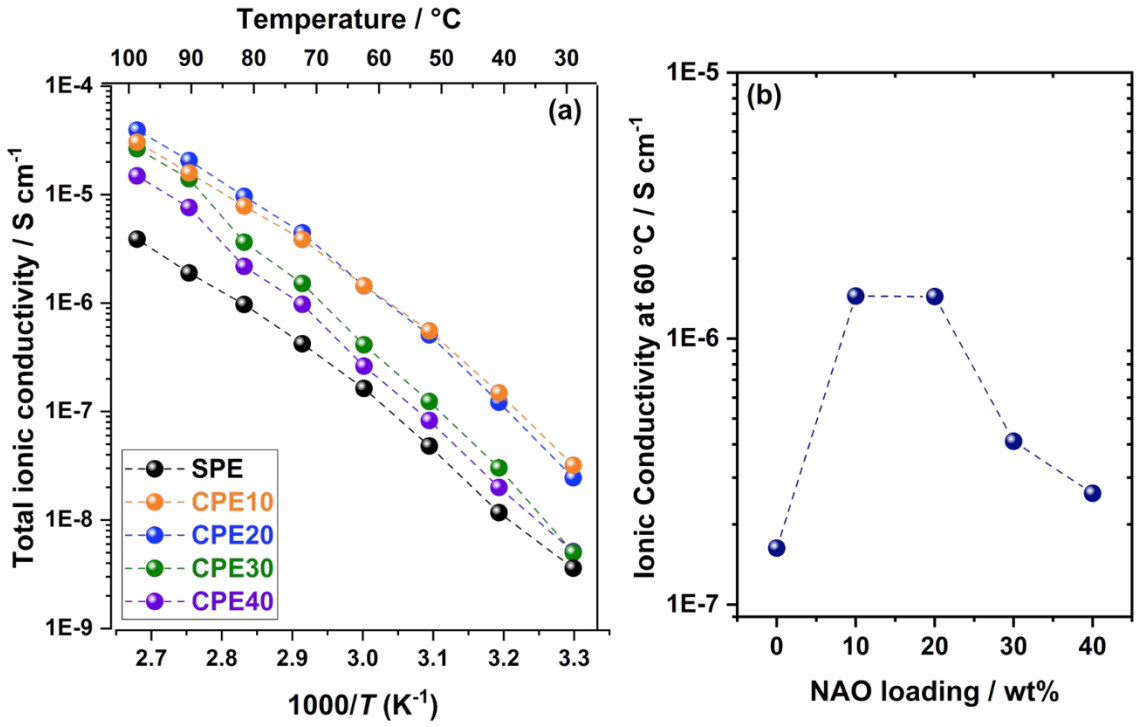

Figure 3. (a) Total ionic conductivity as a function of temperature for the filler-free reference SPE and NAO-based CPEs within a temperature range from 30 up to 90 °C; (b) ionic conductivity as a function of the ceramic filler concentration at 60 °C.

Based on the ionic conductivity data, the CPE at 20 wt.% of NAO particles (denoted as CPE20NAO) exhibits the highest ionic conductivity in large parts of the explored temperature range, and was therefore chosen for measurement of the Na^+ transference number. While the Bruce–Vincent method is relatively easily employed for Li systems, the experiment is much more challenging for Na systems because of the difficulty to reach a stable steady-state current after polarization due to instability at the interface between the electrolyte and sodium metal.[41] While it was indeed difficult to properly determine the T_+ from the filler-free SPE due to such instabilities, the CPE20NAO successfully enables a sufficient interfacial stability against Na metal. As displayed in **Figure 4,** a steady-state current is reached after 80 min from polarizing the cell potentiostatically, and using Equation 1, a Na^+ transference number of 0.92 at 60 °C was determined for the CPE at 20 wt.% of NAO particles. This value far exceeds the T_+ reported for the PTMC:LiTFSI SPE (~0.8 at 60 °C),[42] and is also higher than for a PTMC-based SPE with NaFSI (~0.48 at 80 °C).[15] This is by far the highest transference number reported for a PTMC-based Na-conducting electrolyte, and is consistent with the T_+ obtained for the PTMC:LiTFSI-based CPE with LAO particles.[27]

View Article Online
DOI: 10.1039/D5TA03403E

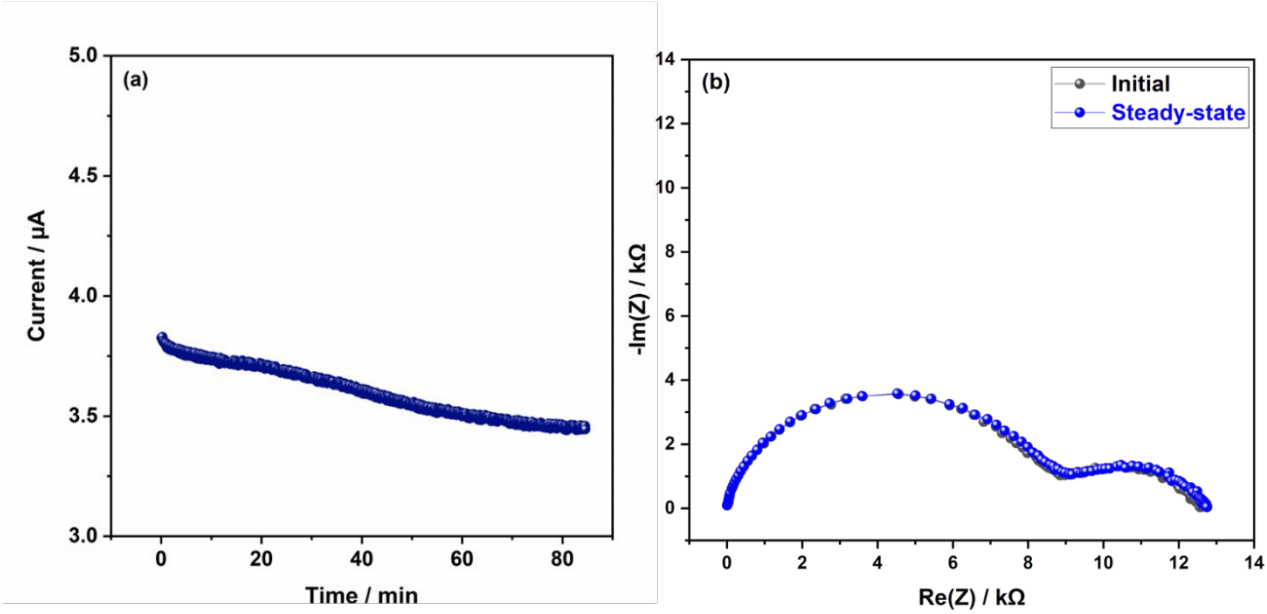

Figure 4. (a) Chronoamperogram of CPE20 in a Na-metal symmetrical cell; (b) Nyquist plot of the same cell obtained before and after polarization. The interfacial resistance is determined after fitting using an appropriate equivalent circuit.[28] The experiment was carried out at 60 °C.

The clear improvement of the Na^+ conduction in the NAO-containing CPEs should also be beneficial for use in Na-metal battery cells. To this end, the CPE with 20 wt.% of NAO particles was employed in solid-state Na-metal batteries, composed of a Prussian white cathode, a Na metal anode, and the CPE20NAO electrolyte. When applying a gentle pressure over the pouch cell, promising electrochemical performance of CPE20NAO in fully solid-state Na-metal batteries could be achieved at a C-rate of C/10 and at an operating temperature of 55 °C, as can be seen in **Figure 5**. An initial capacity of 145 mAh g^{-1} was recorded while the initial coulombic efficiency was above 99%. It is noticed that few scattered datapoints are observed during cycling, which can be explained by a possible occurrence of side reactions due to sodium salt decomposition.[43] However, the incorporation of NAO particles is most likely contributing to inhibit side reactions through stabilization of the sodium salt through a similar effect as previously observed for the

View Article Online
DOI: 10.1039/D5TA03403E

LAO-based CPEs.[27] After 200 cycles, 54% of the initial capacity was retained with a coulombic efficiency at ca. 99%.

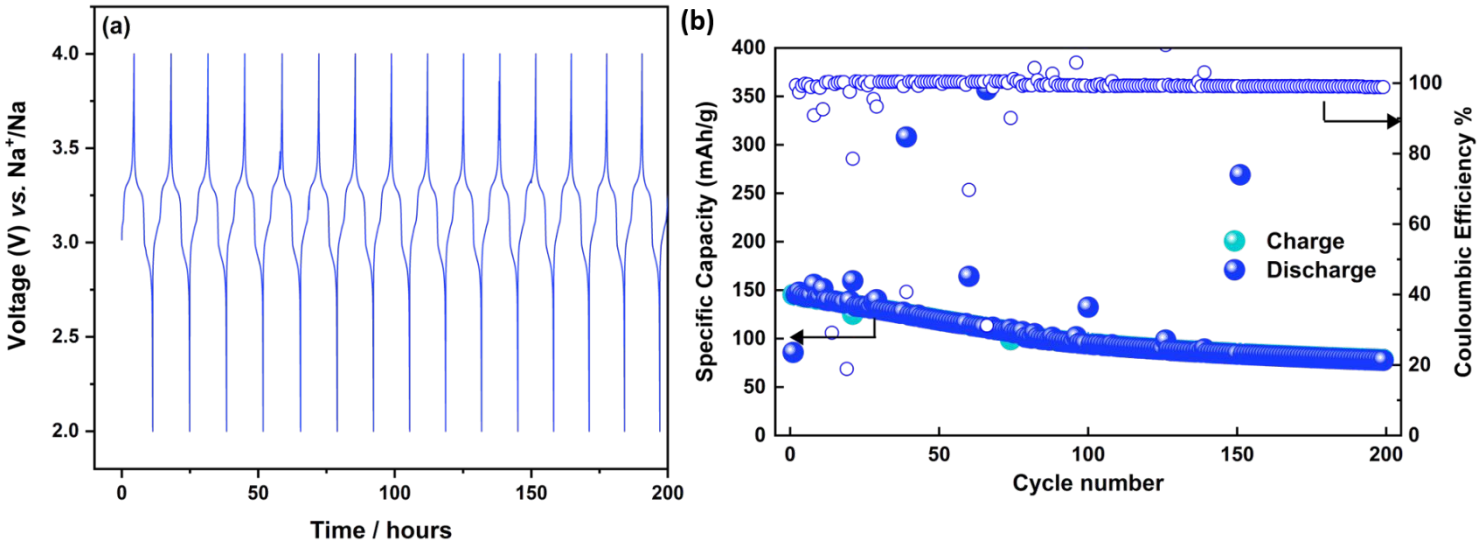

Figure 5. (a) Voltage profile; (b) Cycling performance (specific capacity and coulombic efficiency) of a Na|CPE20NAO|$Na_xFe[Fe(CN)_6]$ solid-state battery cell cycled at C/10 at 55 °C, within the voltage window of 2.0 – 4.0 V.

To improve capacity, rate-performance and room temperature performance, an approach of wetting with liquid electrolytes was employed to ensure better interfacial contacts between the electrodes and electrolyte than in a full solid-state configuration. Thereby, a battery cell in pouch cell configuration was assembled, composed of a Prussian white cathode, a Na metal anode, and the CPE20NAO electrolyte to which 40 µL of 1 M NaFSI in EC:DEC (vol 1:1) was added. Galvanostatic cycling was carried out at an initial C-rate of C/10 and at room temperature, and an initial capacity of ~ 143 mAh g^{-1} and a coulombic efficiency of 97.5% were recorded. The Na-metal battery cell displayed stable cycling, as seen in **Fig. 6a**, indicating the formation of stable electrolyte/electrode interphases that circumvents the occurrence of side reactions. In previously reported studies on PTMC-based SPE with a Na salt, erratic cell behavior has been observed due to salt decomposition and associated to parasitic reactions.[15] The results here thus further suggest that there is a positive effect on the electrochemical stability of the PTMC-based SPE when NAO particles are incorporated. Furthermore, the rate performance of CPE20NAO in Na-metal batteries was evaluated by cycling the battery while increasing the C-rate up to 5C. As shown in **Fig. 6b**, the cell capacity is gradually decreasing with increasing C-rate, however, the battery cell shows a fairly high capacity at all rates, being higher than ~ 92 mAh g^{-1} even at 5C.

View Article Online
DOI: 10.1039/D5TA03403E

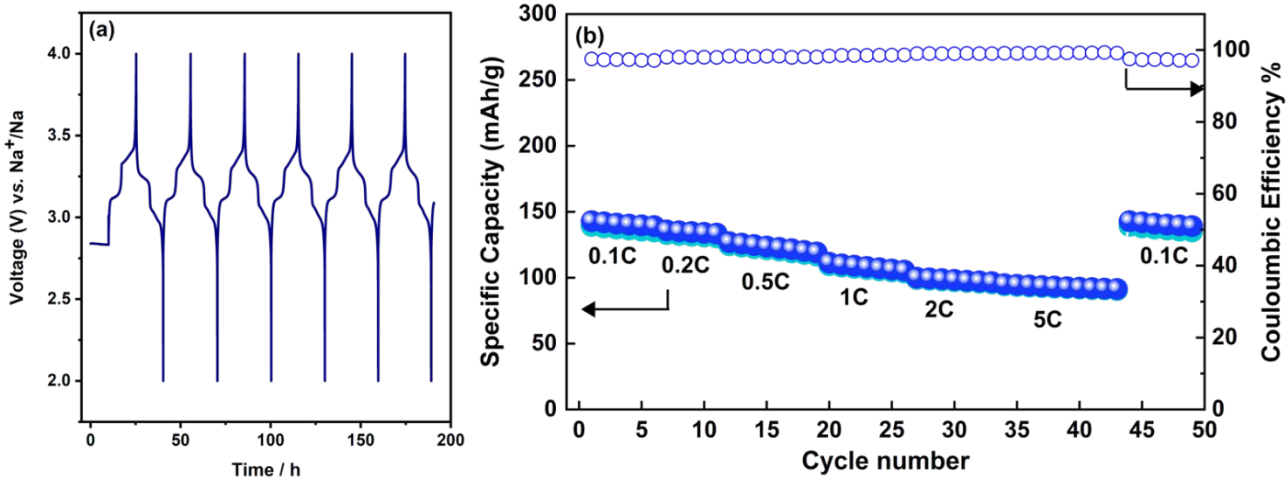

Figure 6. (a) Voltage profile of CPE20NAO in a battery cell comprising Prussian white positive electrode and Na metal negative electrode cycled at C/10 at room temperature with some drops of liquid electrolyte added; (b) Specific capacity and coulombic efficiency of the same battery cell recorded with increasing the C-rate from C/10 up to 5C within the voltage window of 2.0 – 4.0 V and at room temperature.

It is important to note that the possibility of cycling such a battery cell at room temperature and at high C-rates is dependent on the addition of liquid electrolyte, which also plasticizes the SPE and enables a lower resistivity of the CPE. However, these additives can be consumed by interfacial reactions with the electrode materials during long-term operation, causing battery failure or instabilities. Therefore, the interfacial electrode/electrolyte should be improved by means of a different strategy other than liquid electrolyte wetting, and further solid-state cell engineering techniques are necessary, e.g. use of oligomeric coatings and tailoring of the electrode composition, porosity and the applied pressure. Nevertheless, the results indicate that it is not primarily the bulk conductivity of the solid-state CPE materials which is the main hurdle for successful battery operation, but rather the interfacial properties between the electrode and electrolyte – most likely on the cathode side – and which is facilitated by the addition of small amounts of liquid. That the plateaus in the galvanostatic cycling date are clearly visible and located at the same voltages in **Fig. 5a** and **Fig. 6a** indicate the functionality of the solid-state electrolyte. These results thereby open the door towards further optimization of the battery design and composition to realize CPEs for solid-state Na-metal batteries.

Conclusions

In this work, we demonstrate the potential of implementing a polycarbonate-based composite electrolyte with the non-conductive $NaAlO_2$ ceramic filler for solid-state Na-metal batteries. It is shown that the ionic conductivity and cationic transference number are significantly improved as compared to the filler-free system, analogous to the equivalent Li-based system. Moreover, the fillers render a mechanically more robust electrolyte, facilitating the implementation of the materials into functional Na battery cells using sustainable materials throughout. Such CPE-based

View Article Online
DOI: 10.1039/D5TA03403E

solid-state battery cells cycled reliably for hundreds of cycles at elevated temperatures. Overall, this study opens up for further exploration of similar CPE platforms for Na-based solid-state batteries.

Acknowledgments

This work was supported by the European Research Council (ERC) under the European Horizon 2020 research and innovation programme (Grant agreement No. 771777 FUN POLYSTORE), the Swedish Foundation for Strategic Research (project SOLID ALIBI, grant no. ST19-0095), the Swedish Research Council (grant no. 2024-05180) and STandUP for Energy. Ida Nielsen, Luca Peters, Svea Schlag and Karen Palabral at Uppsala University are acknowledged for assistance with XRD refinement, synthesis of $NaAlO_2$, fabrication of CPE films and SEM imaging, respectively.

References

1 V. Palomares, P. Serras, I. Villaluenga, K. B. Hueso, J. Carretero-González and T. Rojo, *Energy Environ. Sci.*, 2012, **5**, 5884.
2 T.Y. Kim, T. Gould, S. Bennet, F. Briens, A. Dasgupta, P. Gonzales, A. Gouy, G. Kamiya, M. Karpiniski and J. Lagelee, *Int. Energy Agency Washington, DC, USA*, 2021, 70–71.
3 T. Schmaltz, F. Hartmann, T. Wicke, L. Weymann, C. Neef and J. Janek, *Adv. Energy Mater.*, 2023, **13,** 43.
4 J. Janek and W. G. Zeier, *Nat. Energy*, 2023, **8**, 230–240.
5 Y. Dong, P. Wen, H. Shi, Y. Yu and Z. Wu, *Adv. Funct. Mater.*, 2024, **34**, 5.
6 K. Edström, J. O. Thomas and G. C. Farrington, *Acta Crystallogr. Sect. B Struct. Sci.*, 1991, **47**, 210–216.
7 T. Wu, Z. Wen, C. Sun, X. Wu, S. Zhang and J. Yang, *J. Mater. Chem. A*, 2018, **6**, 12623–12629.
8 C. Wang, H. Jin and Y. Zhao, *Small*, 2021, **17**, 23.
9 H.P. Hong, *Mater. Res. Bull.*, 1976, **11**, 173–182.
10 A. Hayashi, K. Noi, A. Sakuda and M. Tatsumisago, *Nat. Commun.*, 2012, **3**, 856.
11 A. Banerjee, K. H. Park, J. W. Heo, Y. J. Nam, C. K. Moon, S. M. Oh, S. Hong and Y. S. Jung, *Angew. Chemie Int. Ed.*, 2016, **55**, 9634–9638.
12 Z. Sun, M. Liu, Y. Zhu, R. Xu, Z. Chen, P. Zhang, Z. Lu, P. Wang and C. Wang, *Sustainability*, 2022, **14**, 9090.
13 X. Qi, Q. Ma, L. Liu, Y. Hu, H. Li, Z. Zhou, X. Huang and L. Chen, *ChemElectroChem*, 2016, **3**, 1741–1745.
14 C. Sångeland, R. Younesi, J. Mindemark and D. Brandell, *Energy Storage Mater.*, 2019, **19**, 31–38.
15 C. Sångeland, R. Mogensen, D. Brandell and J. Mindemark, *ACS Appl. Polym. Mater.*, 2019, **1**, 825–832.
16 E. Ruoff, S. Kmiec and A. Manthiram, *Small*, 2024, **20**, 24.
17 J. Yang, H. Zhang, Q. Zhou, H. Qu, T. Dong, M. Zhang, B. Tang, J. Zhang and G. Cui, *ACS Appl. Mater. Interfaces*, 2019, **11**, 17109–17127.
18 K. Hiraoka, M. Kato, T. Kobayashi and S. Seki, *J. Phys. Chem. C*, 2020, **124**, 21948–21956.

View Article Online
DOI: 10.1039/D5TA03403E

19 Z. Zhang, Q. Zhang, C. Ren, F. Luo, Q. Ma, Y.-S. Hu, Z. Zhou, H. Li, X. Huang and L. Chen, *J. Mater. Chem. A*, 2016, **4**, 15823–15828.
20 Z. Zhang, K. Xu, X. Rong, Y.-S. Hu, H. Li, X. Huang and L. Chen, *J. Power Sources*, 2017, **372**, 270–275.
21 L. Shen, S. Deng, R. Jiang, G. Liu, J. Yang and X. Yao, *Energy Storage Mater.*, 2022, **46**, 175–181.
22 A. Chandra, A. Chandra and K. Thakur, *Arab. J. Chem.*, 2016, **9**, 400–407.
23 S. Song, M. Kotobuki, F. Zheng, C. Xu, S. V. Savilov, N. Hu, L. Lu, Y. Wang and W. D. Z. Li, *J. Mater. Chem. A*, 2017, **5**, 6424–6431.
24 A. Dey, T. Ghoshal, S. Karan and S. K. De, *J. Appl. Phys.*, 1996, **79**, 8, 5641-5643.
25 T. K. Lee, R. Andersson, N. A. Dzulkurnain, G. Hernández, J. Mindemark and D. Brandell, *Batter. Supercaps*, 2021, **4**, 653–662.
26 J. Serra Moreno, M. Armand, M. B. Berman, S. G. Greenbaum, B. Scrosati and S. Panero, *J. Power Sources*, 2014, **248**, 695–702.
27 K. Elbouazzaoui, A. Mahun, V. Shabikova, L. Rubatat, K. Edström, J. Mindemark and D. Brandell, *Adv. Energy Mater.*, 2025.
28 K. Elbouazzaoui, F. Nkosi, D. Brandell, J. Mindemark and K. Edström, *Electrochim. Acta*, 2023, **462**, 142785.
29 A. A. Coelho, *J. Appl. Crystallogr.*, 2018, **51**, 210–218.
30 J. Evans, C. A. Vincent and P. G. Bruce, *Polymer.*, 1987, **28**, 2324–2328.
31 I. Nielsen, A. Ulander, F. Juranyi, S.R. Larsen, M. Karlsson, W.R. Brant, *Chem. Mater.*, 2024, **36**, 22, 11246-11253.
32 T. Wan, P. Yu, S. Wang and Y. Luo, *Energy & Fuels*, 2009, **23**, 1089–1092.
33 R. Dhanusha, P. M. Srinivasappa, S. C. Alla, M. Hemavathi, D. Prasad, N. K. Chaudhari and A. H. Jadhav, *Appl. Organomet. Chem.*, 2024, **38**, 5.
34 N. V. Proskurnina, V. I. Voronin, G. S. Shekhtman and N. A. Kabanova, *Ionics.*, 2020, **26**, 2917–2926.
35 J. Thery and D. Briancon, *Rev. Int. Hautes Temper. Refract*, 1964, **1**, 221–227.
36 A. R. West, *Nature*, 1974, **249**, 245–246.
37 I. E. Grey, R. J. Hill and A. W. Hewat, *Zeitschrift für Krist.*, 1990, **193**, 51–69.
38 K. Kinoshita, J. W. Sim and J. P. Ackerman, *Mater. Res. Bull.*, 1978, **13**, 445–455.
39 B. Sun, J. Mindemark, E. V. Morozov, L. T. Costa, M. Bergman, P. Johansson, Y. Fang, I. Furó and D. Brandell, *Phys. Chem. Chem. Phys.*, 2016, **18**, 9504–9513.
40 J. Mindemark, R. Mogensen, M. J. Smith, M. M. Silva and D. Brandell, *Electrochem. commun.*, 2017, **77**, 58–61.
41 D. S. Tchitchekova, D. Monti, P. Johansson, F. Bardé, A. Randon-Vitanova, M. R. Palacín and A. Ponrouch, *J. Electrochem. Soc.*, 2017, **164**, A1384–A1392.
42 B. Sun, J. Mindemark, K. Edström and D. Brandell, *Solid State Ionics*, 2013, 2–6.
43 K. Pfeifer, S. Arnold, J. Becherer, C. Das, J. Maibach, H. Ehrenberg and S. Dsoke, *ChemSusChem*, 2019, **12**, 3312–3319.

View Article Online
DOI: 10.1039/D5TA03403E

Data sharing statement

All research data for the article is deposited at Zenodo and publically available: https://doi.org/10.5281/zenodo.15305469